J Clust Sci (2017) 28:2503–2516
DOI 10.1007/s10876-017-1242-9

ORIGINAL PAPER

Structural, Relative Stable, and Electronic Properties of Pb_nSn_n (n = 2–12) Clusters were Investigated Using Density Functional Theory

Gao-feng Li[2,3] · Zhi-qiang Zhou[1,2,3] · Xiu-min Chen[1,2,3] · Jia-ju Wang[2,3] · Hong-wei Yang[2,3] · Bin Yang[2,3] · Bao-qiang Xu[2,3] · Da-chun Liu[2,3]

Received: 12 January 2017 / Published online: 19 May 2017

Abstract The structural, relative stable and electronic properties of Pb_nSn_n (n = 2–12) alloy clusters were systematically studied using density functional theory. The isomers of Pb_nSn_n alloy clusters were generated and determined by ab initio molecular dynamics. By comparing the calculated parameters of Pb_2 dimer and Sn_2 dimers with the parameters from experiments, our calculations are reasonable. With the lowest-energy structures for Pb_nSn_n clusters, the average binding energies, fragmentation energies, second- order energy differences, vertical ionization potentials, vertical electron affinities, HOMO–LUMO gaps, and density of states were calculated and analyzed. The results indicate that the Sn atoms have a tendency to bond together, the average binding energies tend to be stable up to n = 8, Pb_8Sn_8 cluster is a good candidate to calculate the molecular interaction energy parameter in Wilson equation, the clusters become less chemical stable and show an insulator-to-metallic transition, 3, 6, 8 and 11 are magic numbers of Pb_nSn_n (n = 2–12) clusters, the charges always transfer from Sn atoms to Pb atoms in Pb_nSn_n clusters except for $Pb_{10}Sn_{10}$ cluster, and density of states of Pb_nSn_n clusters becoming continuous and shifting toward negative with the increasing size n.

Keywords Clusters · Density of states · Ab initio molecular dynamics · Lowest-energy structures · Atoms

✉ Xiu-min Chen
chenxiumin9@hotmail.com

[1] State Key Laboratory of Complex Nonferrous Metal Resources Clear Utilization, Kunming University of Science and Technology, Kunming 650093, People's Republic of China

[2] National Engineering Laboratory for Vacuum Metallurgy, Kunming University of Science and Technology, Kunming 650093, People's Republic of China

[3] Yunnan Provincial Key Laboratory for Nonferrous Vacuum Metallurgy, Kunming University of Science and Technology, Kunming 650093, People's Republic of China

Introduction

Clusters demonstrate excellent catalytic [1, 2], adsorbent [3, 4], magnetic [5, 6], sensing [7, 8] and optical [9, 10] properties, etc. The investigation of clusters is a fundamental study but it's very important and interesting, because the fundamental investigation can accelerate our steps on understanding the novel properties of cluster-assembled materials at atomic scale [11, 12]. As we all know, the properties of nanomaterials depend on its micro-structures and electronic structures essentially [13]. Then, the investigations of structural and electronic properties of clusters on particular materials are essential, which may facilitate the design of new materials with novel properties. However, some difficulties ahead of us, determining the structural and electronic properties of nanomaterials by experiments are of great difficult [14]. But the study on theoretical calculation is a good method due to the calculated results can provide reasonable results compared with the experimental data at a certain extent. Currently, the structural, relative stable and electronic studies of alloy clusters using density functional theory have attracted many scholar's attention from all over the world.

Pb is harmful to human health and legislations have been established by government to prevent people from Pb. However, the Pb-containing solders are widely used in the world, which poses great threat to people's health. The low-cost and accessible Pb-free solders are receiving increased attention from the material community. Then, the properties of Pb_nSn_n clusters would provide very important information for the Pb-containing solders and the materials to replace harmful Pb in Pb-containing solders. Moreover, the candidate Pb_nSn_n clusters can be used to calculate the molecular interaction energy parameters in the Wilson equation which can be used to calculate the phase diagram of vapor–liquid equilibria (VLE) [15, 16].

The pure Sn_n clusters and Pb_n clusters were investigated extensively. With the experimental and theoretical investigations on Sn_n Clusters and Pb_n clusters, the results show that these clusters show insulator-to-metallic transitions [17–20]. As the size n of Sn_n clusters and Pb_n clusters increasing, the properties of those clusters convergence to the bulk state [21]. Osmekhin et al. [17] applied the photoelectron spectroscopy to study free nanoscale Sn_n clusters in the size n ranged from a few tens to 500 atoms, and the metal-to-semiconductor transition was discovered. Majumder et al. [22–24] systematically investigated ground-state structures of neutral and cation Sn_n clusters ($n \leq 20$), the results show that growth behavior of Sn_n clusters is different from Si_n clusters and Ge_n clusters at $n \geq 8$ but some of them are similar, and the vertical ionization potentials and fragmentation behavior of Sn_n clusters are in accordance with experimental results. Bachels et al. [25] determined a formation enthalpy per atom of Sn_n clusters with the average size of $n = 150$. Saito et al. [26] investigated the relative abundance of Pb_n clusters using time-of-flight mass spectrometer and electron bombardment, the results show the size n of the clusters up to ten atoms were observed and Pb_7 cluster shows the highest intensity. Tchaplyguine et al. [18] and Bahn et al. [19] applied 4f and 5d photoelectron spectroscopy to investigate neutral and anionic Pb_n clusters are in the

range of 10–100, the results show that with the increasing size n of Pb_n clusters, the non-metallic to metallic transition was observed. Whereas, Wang et al. [20] systematically calculated the Pb_n (n = 2–22) clusters using DFT, the covalent to metallic transition was also found. Majesh et al. [27] investigated the atomic and electronic properties of Pb_n (n = 2–15) and Pb_n^+ (n = 2–15) clusters by density functional theory, the results show that the cationic and neutral clusters show similar growth patterns, and 4, 7, 10 and 13 are the magic numbers. Li et al. [28] calculated the neutral Pb_n (n = 21–30) clusters using first principle calculation, the results show that $Pb_{22–26}$ clusters favor endohedral cage structures and $Pb_{27–30}$ clusters prefer three endohedral structures, and 24 and 28 are the magic numbers.

The Sn-based alloy clusters and Pb-based alloy clusters were also aroused much interest due to the properties of the alloy clusters are different from the pure metallic clusters. Sosa-Hernández et al. [29] reported the lowest-energy isomers and magnetic properties and stabilities of Co_xSn_y clusters ($x + y \leq 5$) using density functional theory, they found that the geometries are significantly different to the pure clusters, the magnetic behavior is independent of the concentration of Co and the mixing of bimetallic clusters are favorable. Samanta et al. [30] studied the structures, binding and electronic properties of Sn_mGe_n ($m + n \leq 5$) clusters with density functional theory, the results would provide some fundamental theory for the mechanism of CO oxidation on Sn_mGe_n clusters. Sosa-Hernández et al. [31] adopted density functional theory to study the structural and electronic properties of Fe_xSn_y ($x + y \leq 5$) clusters, they found that the binary clusters are different from the pure clusters, the magnetic properties are not related with the Fe concentration. Tai et al. [32] reported small Sn_nZn (n = 1–12) with DFT and CCSD methods, the results show that impurity Zn atom on the surface of Sn_n clusters, the Zn atom is encapsulated into the empty cages of Sn_n clusters with n = 11 and n = 12, the transition appears at n = 9 and n = 10, and $Sn_{12}Zn$ cluster and $Sn_{10}Zn$ cluster are the magic clusters. Paz-Borbón et al. [33] investigated hydrogenation of C_2H_4 to C_2H_6 over Ru_N clusters and $(RuSn)_N$ clusters with density functional theory, the results show that the $(RuSn)_N$ clusters have pronounced effects on the hydrogenation compared with Ru_N clusters, Ru_N clusters adopt cubic conformations while $(RuSn)_N$ clusters prefer compact Ru cores capped by Sn atoms. Melko et al. [34] studied the structural and electronic properties of $Pb_xSb_y^-$ clusters and $Sn_xBi_y^-$ clusters combined photoelectron spectroscopy with DFT, the results show that the clusters may not be the excellent building blocks,but qualified for the applications in energetic, electronic and optical function. Xing et al. [35] investigated the magic numbers of $(M/Pb)^-$ (M = Au, Ag and Cu) clusters by laser ablation and ToF-MS, they found that most of the magic clusters can be explained by electron shell models. Melko et al. [36] investigated the structural and electronic properties of neutral and anionic Pb_xIn_y ($x \leq 5$, $y \leq 7$) clusters by photoelectron spectroscopy and DFT, the results show that stabilities of some clusters were enhanced, which can provide valuable guidances for cluster-assembled materials. Rajesh et al. [37] systematically investigated the effects of impurity atoms on Pb_nM (M = C, Al, In, Mg, Sr and Ba) clusters with first principle calculations, the results reveal that the location of impurity atom on Pb_nM cluster depends on atomic radius of the impurity atom and the interactions between the host cluster and the impurity atom, Mg atom

lowers the stabilities of Pb_n clusters while C and Al enhance the stability. Barman et al. [38] systematically studied the structural and electronic properties of $Pb_{n-1}Sn$ clusters and $Sn_{n-1}Pb$ clusters with first principle calculations, the results show that dopant Pb atom lowers the stabilities of $Sn_{n-1}Pb$ clusters while dopant Sn atom enhances the stabilities of $Pb_{n-1}Sn$ clusters, 4, 7, 10 and 12 are the magic numbers of $Sn_{n-1}Pb$ clusters and 4, 7 and 9 are the magic numbers of $Pb_{n-1}Sn$ clusters. Orel et al [39] studied the geometries, relative energies and electronic properties of global minima of Sn_mPb_n ($7 \leq m + n \leq 12$) clusters, generally, the calculated results are excellent agreement with experimental data.

Although the structural and electronic properties of Sn_n clusters, Pb_n clusters, Sn-based clusters and Pb-based clusters were extensive investigated by density functional theory and experimental investigations. The Pb_nSn_n clusters were scarcely reported, we believe that our work is meaningful. In this paper, we will focus our attention on the structural, relative stable and electronic properties of Pb_nSn_n (n = 2–12) clusters using density functional theory.

Computational Methods

In this work, all the density functional theory calculations were carried out in $DMol^3$ package [20, 40]. In order to ignore the effects of the initio structures, the isomers of Pb_nSn_n clusters were extensively generated by ab initio molecular dynamics. During the dynamics calculation, the temperature maintains at 300 K, 1 ps for each time step, total simulation time is 100 ps. The GGA [40]-BLYP [20] was used to treat the exchange-correlation functional. The core was treated by DFT semi-core potential. Basis set was treated by double numerical basis with polarized functions (DNP) [20, 40]. The different spin multiplicities were taken into consideration in the geometric optimization processes. A SCF convergence criterion is 10^{-6} Ha on the total energy. With respect to density mixing standard, 0.2 and 0.5 are for charge and spin, respectively. In order to obtain a good convergence result, the smearing was used and its value is 0.005 Ha. Energy convergence is 10^{-5} Ha per atom and that of maximum force is 0.002 Ha/Å. The maximum displacement is less than 0.005 Å.

The parameters of Pb_2 dimer and Sn_2 dimer were calculated to verify the computational schematic processes, whereas the experimental parameters of the dimers were achieved from literature, the detailed information are shown in Table 1. Comparing the calculated and experimental data, we can clearly see that the

Table 1 Bond lengths (R), binding energies (E_b), frequencies (ω) and vertical ionization potentials (VIP) of Pb_2 dimer and Sn_2 dimer are from calculations and experiments

	R/(Å)	E_b/(eV)	ω/(cm^{-1})	VIP/(eV)
Expt. for Sn_2 dimer	2.75 [41]	0.94 [24]	189.73 [41]	7.06–7.24 [42]
This work for Sn_2 dimer	2.85	0.98	151.72	6.70
Expt. for Pb_2 dimer	3.07 [20]	1.43 [20]	111.10 [20]	6.20 [26]
This work for Pb_2 dimer	3.01	1.10	114.95	6.35

calculated data are excellent agreement with experimental data. It is obvious that our computational methods are reliable.

Results and Discussion

The ground-state structures of Pb_nSn_n clusters are shown in Fig. 1. From Fig. 1, we can see that the Pb_2Sn_2 cluster is in the shape of distorted parallelogram which two Sn atoms on the same side, and its point group symmetry is C_s. The ground-state structures of Pb_4 cluster and Sn_4 cluster are also parallelogram structures [21, 43]. The Pb_3Sn_3 cluster is a bipyramid with C_{2v} symmetry, the three Sn atoms on the same plane. It is interesting to note that the Pb_2Sn_2 cluster is a planar structure while the Pb_3Sn_3 cluster is a three dimensional structure, the Pb_nSn_n clusters show a planar structure to three dimensional structure transition. Additionally, the similar transition was also observed in Sn_n clusters from Sn_4 cluster to Sn_6 cluster and that of Pb_n clusters from Pb_4 cluster to Pb_6 cluster [21, 43]. The Pb_4Sn_4 cluster is an inclined four prism without any symmetry. Furthermore, the Pb_nSn_n clusters are don't show any symmetry from $n = 4$ to $n = 12$, which could reduce the total energies of the clusters and make the clusters more stable [44]. The structure of Pb_5Sn_5 cluster is similar with that of Pb_4Sn_4 cluster by capped one Pb atom and one Sn atom. Pb_6Sn_6 cluster can be regarded as a bi-layer structure. From $n = 7$ to $n = 12$, the shapes of the clusters are ellipsoid and the positions of Pb atoms and Sn atoms are out of order, but the Sn atoms tend to gather together. In addition, the characteristic frequencies show a oscillator for Pb_nSn_n clusters in the range of $n = 2$–8, whereas for $n = 8$–12, the characteristic frequencies decrease with increasing size n except for $Pb_{12}Sn_{12}$ Cluster. This may be related to the ground state structures of Pb_nSn_n ($n = 2$–12) clusters.

The binding energies per atom of lowest-energy structures of Pb_nSn_n clusters can be defined as [39, 45–51]

$$E_b = [nE(Sn) + nE(Pb) - E(Pb_nSn_n)]/2n$$

where E(Sn), E(Pb) and $E(Pb_nSn_n)$ are energies of Sn atom, Pb atom and Pb_nSn_n clusters, respectively. The average binding energies (E_b) of Pb_nSn_n ($n = 2$–12) clusters are shown in Fig. 2. Binding energy can reflect the thermodynamic stabilities

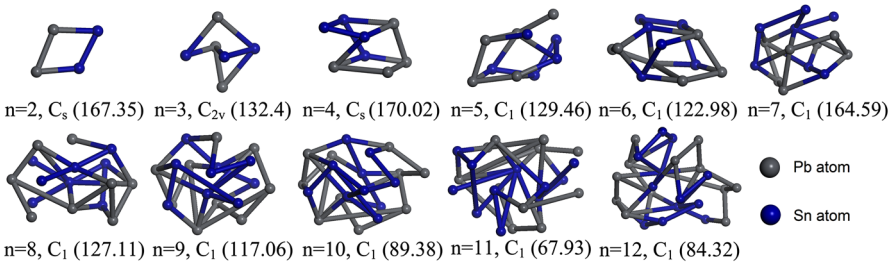

Fig. 1 Ground-state structures and point groups of Pb_nSn_n ($n = 2$–12) clusters (corresponding characteristic frequencies are in the parentheses)

of clusters. From Fig. 2, the average binding energies increase with the increasing size n, then it tend to be stable up to n = 8. The similar trend of binding energies were also observed in pure Sn_n clusters [24] and pure Pb_n clusters [20]. It suggests that the thermodynamic stabilities of Pb_nSn_n clusters increase and the stabilities tend to be stable when n up to 8. It is concluded that Pb_nSn_n ($n \geq 8$) clusters are the ideal candidates to calculate the molecular interaction energy parameter in phase diagram of vapor–liquid equilibria (VLE) [15]. The slope between Pb_2Sn_2 cluster and Pb_3Sn_3 cluster shows steep increase which means the compactness of Pb_3Sn_3 cluster are better than Pb_2Sn_2 cluster. In addition, it is originated from the transition from a planar structure to a three dimensional structure.

The fragmentation energies (ΔE) and second-order energy differences ($\Delta_2 E$) can be defined as [46, 52–54]

$$\Delta E(PbSn)_n = E(PbSn)_{n-1} + E(PbSn) - E(PbSn)_n$$

$$\Delta_2 E(PbSn)_n = E(PbSn)_{n+1} + E(PbSn)_{n-1} - E(PbSn)_n$$

where $E(PbSn)_{n-1}$, $E(PbSn)$, $E(PbSn)_n$ and $E(PbSn)_{n+1}$ represent the energies of $Pb_{n-1}Sn_{n-1}$ cluster, PbSn cluster, Pb_nSn_n cluster and $Pb_{n+1}Sn_{n+1}$ cluster, respectively. The ΔE and $\Delta_2 E$ of Pb_nSn_n clusters are presented in Figs. 3 and 4. From Fig. 3, the ΔE of Pb_3Sn_3 cluster, Pb_8Sn_8 cluster and $Pb_{11}Sn_{11}$ cluster have larger values than their neighboring clusters, indicating that the three clusters are more stable than their neighbors. From Fig. 4, the trend of second-order energy differences is excellent agreement with that of second-order energy differences. We also find that Pb_3Sn_3 cluster, Pb_8Sn_8 cluster and $Pb_{11}Sn_{11}$ cluster are higher stabilities than their neighbors.

The vertical ionization potentials of Pb_nSn_n clusters are shown in Fig. 5. Vertical ionization potential is defined as the neutral cluster loses one electron and adsorbs energy to become a positive charged cluster, and the energy can be viewed as the

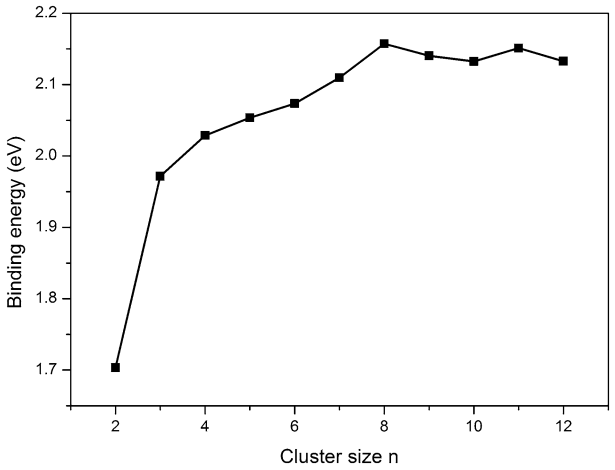

Fig. 2 Average binding energies of Pb_nSn_n (n = 2–12) clusters

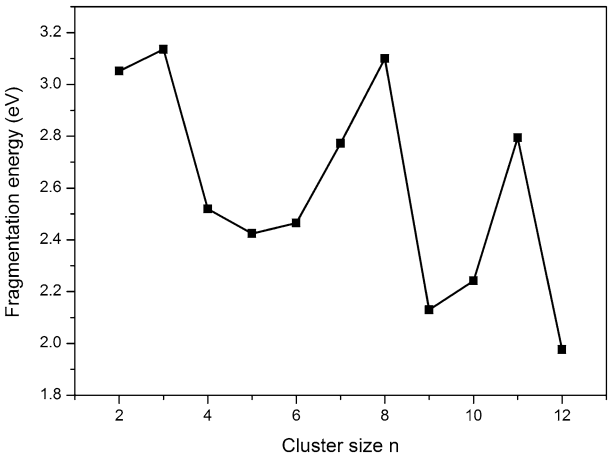

Fig. 3 The ΔE of Pb_nSn_n (n = 2–12) clusters

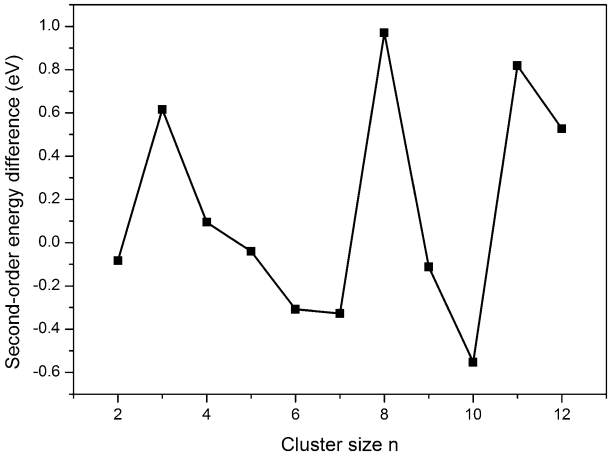

Fig. 4 The Δ_2E of Pb_nSn_n (n = 2–12) clusters

vertical ionization potential [51, 52]. It means that the higher value of vertical ionization potential, the more difficult for the neutral cluster to ionize and becomes a positive cluster. As we can see from Fig. 5, the values of vertical ionization potentials decreasing with the variation of size n, which also show that the Pb_nSn_n clusters become more and more easier to lose one electron and become a positive cluster. Based on the trend, we can refer that metallicity of Pb_nSn_n clusters become more and more stronger.

Vertical electron affinities of Pb_nSn_n clusters are shown in Fig. 6. The vertical electron affinity can reflect the chemical stabilities of the neutral clusters [51, 52]. The higher value of vertical electron affinity, the easier for a neutral cluster to accept one electron and becomes a negative cluster. As it is shown in Fig. 6, the

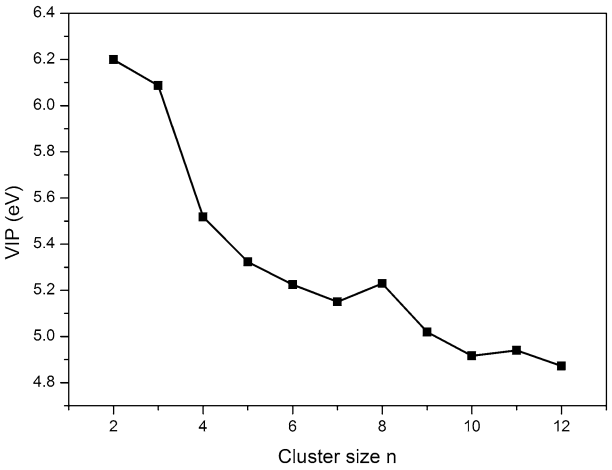

Fig. 5 Vertical ionization potentials (VIP) of Pb_nSn_n (n = 2–12) clusters

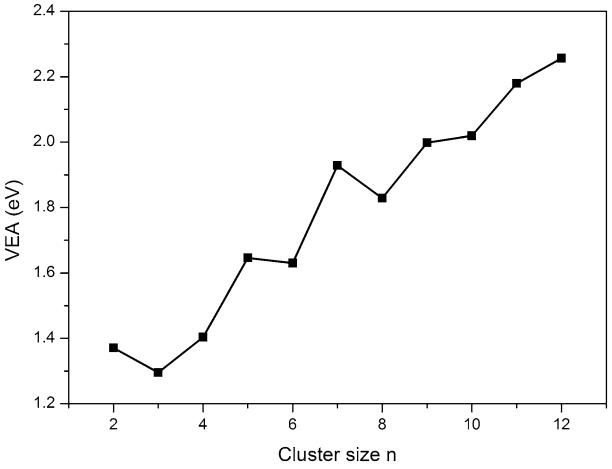

Fig. 6 Vertical electron affinities (VEA) of Pb_nSn_n (n = 2–12) clusters

vertical electron affinities of Pb_nSn_n clusters increase with increasing size n, which means the neutral clusters become more and more easier to accept electrons and become negative clusters.

The HOMO–LUMO gaps of Pb_nSn_n clusters are shown in Fig. 7. The HOMO–LUMO gap (HL gap) can also reflect the chemical stabilities of the clusters [53, 54]. The higher HL gap means the gap between highest occupied molecular orbitals and lowest unoccupied molecular orbitals are larger, which indicates that it is difficult for electrons transfer from conduction band to valence band, and the neutral cluster is more chemically stable. From Fig. 7, there is a general trend that values of HL gaps sharply decrease with the variation of size n, which means the chemical stabilities of Pb_nSn_n clusters also sharply decrease and the trend is excellent

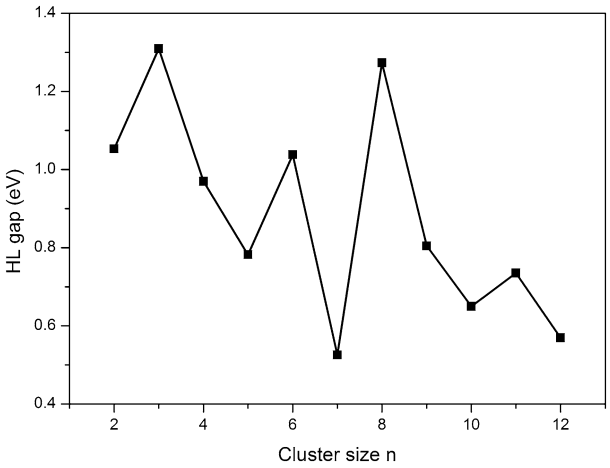

Fig. 7 HOMO–LUMO gaps of Pb_nSn_n (n = 2–12) clusters

agreement with that of VIPs and VEAs. It is also referred that the Pb_nSn_n clusters show a covalent-to-metallic transition in the range of n = 2–12. Moreover, Pure Pb_n clusters and pure Sn_n clusters also show covalent-to-metallic transitions [17, 18]. Compared the transition size n of pure Pb_n clusters and pure Sn_n clusters, the alloy Pb_nSn_n clusters show the transition with smaller size n. It is interesting to note that the values of Pb_3Sn_3 cluster, Pb_6Sn_6 cluster, Pb_8Sn_8 cluster and $Pb_{11}Sn_{11}$ cluster are larger than their neighbors, which means that the Pb_3Sn_3 cluster, Pb_6Sn_6 cluster, Pb_8Sn_8 cluster and $Pb_{11}Sn_{11}$ cluster are more chemically stable than their neighbors and are also excellent agreement with that of the clusters analyzed by VIPs and VEAs. Furthermore, we conclude that 3, 6, 8 and 11 are magic numbers of Pb_nSn_n (n = 2–12) clusters.

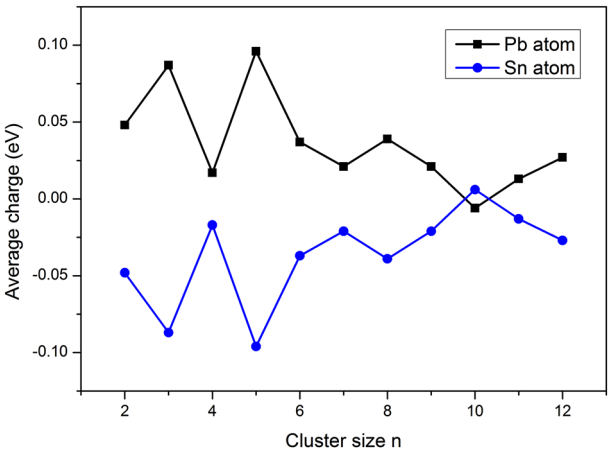

Fig. 8 Average Mülliken charges analysis of Pb_nSn_n (n = 2–12) clusters

The average Mülliken charges are shown in Fig. 8. According to the results, the charges always transfer from Sn atoms to Pb atoms except for $Pb_{10}Sn_{10}$ cluster, which Pb atoms act as electron acceptors while Sn atoms act as electron donators. This situation is similar with that of Sn atoms to Pt atoms in Pt_nSn_n clusters [40] and Al atoms to Ni atoms in Ni_nAl_n clusters [46]. In addition, it is originated from the negativities of element Sn and element Pb (1.96 for Sn and 2.33 for Pb in terms of Pauling's electronegativity scale). There is a trend that the charges decrease with increasing size n, and $Pb_{10}Sn_{10}$ cluster at the turning point, the charges show an odd-even transition up to n = 6 that the clusters with the odd number atoms have less charges transfer than that of the clusters with the even number atoms. It is referred that the Pb_nSn_n clusters may be good catalysts. With respect to the binary Pb–Sn nano-catalysts, the Pb atoms have redundant electrons and would act as active site, whereas those of Sn atoms protect the Pb atoms [40]. From the Fig. 8, Pb_3Sn_3 cluster, Pb_5Sn_5 cluster and Pb_8Sn_8 cluster are located at the local peaks, which imply the strong interactions between Pb atoms and Sn atoms in Pb_3Sn_3 cluster, Pb_5Sn_5 cluster and Pb_8Sn_8 cluster, and they are agreement with the results of fragmentation energies, second-order energy differences and HL gaps.

In order to further explore the electronic properties of Pb_nSn_n clusters, we plotted the density of states of Pb_nSn_n clusters, the details are shown in Fig. 9. The Fermi level is plotted as a vertical dash line and shift to zero. From Fig. 9, we can see that the density of states are mainly consist of two parts, the density of states are between −0.4 to −0.14 Ha and −0.1 to −0.3 Ha, respectively. The density of states between −0.4 and 0.14 Ha are contributed by s electrons and p electrons, which s electrons

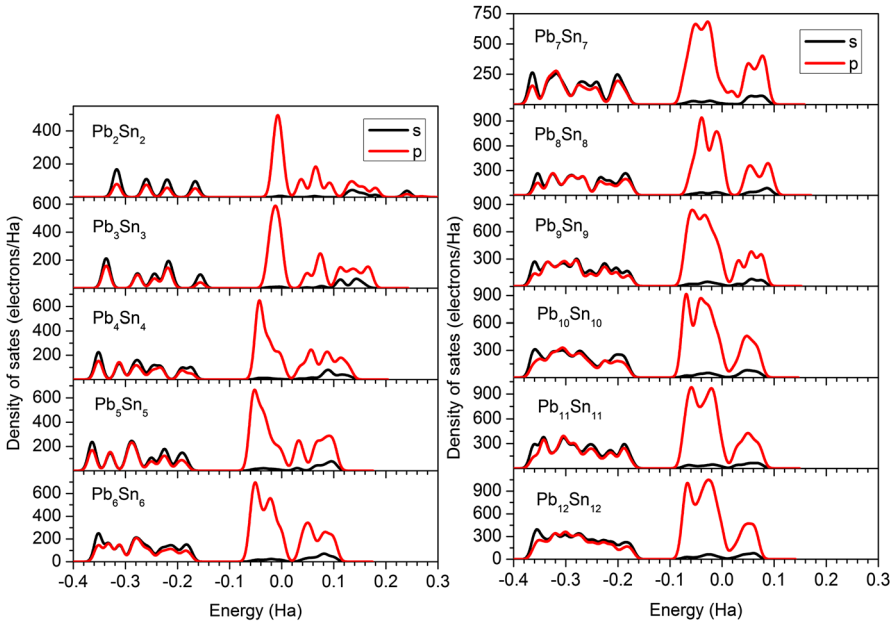

Fig. 9 Density of states of Pb_nSn_n (n = 2–12) clusters

and p electrons almost have the same contributions, while the density of states between −0.1 and 0.3 Ha are contributed by s electrons and p electrons and the contributions within the intervals are mainly contributed by p electrons. Moreover, it is interesting to note that the continuities of the density of states becoming better with the increasing size n, and they shift toward negative and tend to be stable, it may be the reason why the transition from insulator-to-metallic and the clusters become less chemical stable.

Conclusions

We have systematically studied the structural, relative stable and electronic properties of Pb_nSn_n clusters (n = 2–12) using density of states. All the calculations were carried out in DMol^3 package at GGA-BLYP level. According the ground-state structures of Pb_nSn_n clusters, the Sn atoms tend to bond together, and the transition from 2D structure to 3D structure was found. The average binding energies increase with increasing size n, and tend to be stable up to n = 8. Pb_8Sn_8 cluster is a good candidate to calculate the molecular interaction energy parameter for PbSn alloy system. The results of fragmentation energies, second-order energy differences and HOMO–LUMO gaps show that the Pb_3Sn_3 cluster, Pb_6Sn_6 cluster, Pb_8Sn_8 cluster and $Pb_{11}Sn_{11}$ cluster are more stable than their neighbors. The vertical ionization potentials increase with increasing size n while the vertical electron affinities show an opposite trend. The Pb_nSn_n clusters show a covalent-to-metallic transition, and 3, 6, 8 and 11 are the magic numbers of Pb_nSn_n clusters. The charges always transfer from the Sn atoms to Pb atoms except for $Pb_{10}Sn_{10}$ cluster based on the Mülliken charge analysis, which indicate the Pb_nSn_n clusters may be ideal nano-catalysts with controllable properties. The density of states of Pb_nSn_n clusters becoming continuous and shifting toward negative with the increasing size n, which may be the reason why the clusters become less chemical stable and the transition from insulator-to-metallic.

Acknowledgements This work was supported by the Regional Foundation of the National Natural Science Foundation of China (51664032), the Foundation of the State Key Laboratory of Complex Nonferrous Metal Resources Clear Utilization (CNMRCUTS1503), the Joint Foundation of the National Natural Science Foundation of China–Yunnan province (U1502271), the Cultivating Plan Program for the Leader in Science and Technology of Yunnan Province (2014HA003), the Program for Nonferrous Metals Vacuum Metallurgy Innovation Team of Ministry of Science and Technology (2014RA4018) and the National Key Research and Development Program of China (2016YFC0400404).

References

1. C. T. Campbell (2013). The Energetics of Supported Metal Nanoparticles: Relationships to Sintering Rates and Catalytic Activity. *Acc. Chem. Res.* **46**, 1712.
2. H. Zhang, M. Jin, Y. Xiong, B. Lim, and Y. Xia (2013). Shape-Controlled Synthesis of Pd Nanocrystals and Their Catalytic Applications. *Acc. Chem. Res.* **46**, 1783.
3. D. Cortes-Arriagada, M. P. Oyarzun, L. Sanhueza, and A. Toro-Labbe (2015). Binding of Trivalent Arsenic onto the Tetrahedral Au_{20} and $Au_{19}Pt$ Clusters: Implications in Adsorption and Sensing. *J. Phys. Chem. A* **119**, 6909.

4. S. Hirabayashi and M. Ichihashi (2015). NO Decomposition Activated by Preadsorption of O_2 onto Copper Cluster Anions. *J. Phys. Chem. C* **119**, 10850.
5. Z. Ben-Xia, D. Dong, W. Ling, and Y. Ji-Xian (2014). Density functional study on the structural, electronic, and magnetic properties of 3d transition-metal-doped Au_5 clusters. *J. Phys. Chem. A* **118**, 4005.
6. F. Aguilera-Granja, M. B. Torres, A. Vega, and L. C. Balbas (2012). Structural, electronic, and magnetic properties Of Co_nCu_m nanoalloys ($m + n = 12$) from first principles calculations. *J. Phys. Chem. A* **116**, 9353.
7. P. Chen, Y. Li, J. Ma, J. Huang, C. Chen, and H. Chang (2016). Size-tunable copper nanocluster aggregates and their application in hydrogen sulfide sensing on paper-based devices. *Sci. Rep.* **6**, 24882.
8. J. N. Anker, W. P. Hall, O. Lyandres, N. C. Shah, J. Zhao, and R. P. Van Duyne (2008). Biosensing with plasmonic nanosensors. *Nat. Mater.* **7**, 442.
9. W. Ma and F. Chen (2012). Optical and electronic properties of Cu doped Ag clusters. *J. Alloys Compd.* **541**, 79.
10. S. J. Oldenburg, J. B. Jackson, S. L. Westcott, and N. J. Halas (1999). Infrared extinction properties of gold nanoshells. *Appl. Phys. Lett.* **75**, 2897.
11. M. Zhou, C. Zeng, Y. Chen, S. Zhao, M. Y. Sfeir, M. Zhu, and R. Jin (2016). Evolution from the plasmon to exciton state in ligand-protected atomically precise gold nanoparticles. *Nat. Commun.* **7**, 13240.
12. R. Jin, C. Zeng, M. Zhou, and Y. Chen (2016). Atomically Precise Colloidal Metal Nanoclusters and Nanoparticles: Fundamentals and Opportunities. *Chem. Rev.* **116**, 10346.
13. O. Fenwick, E. Coutino-Gonzalez, D. Grandjean, W. Baekelant, F. Richard, S. Bonacchi, D. De Vos, P. Lievens, M. Roeffaers, J. Hofkens, and P. Samori (2016). Tuning the energetics and tailoring the optical properties of silver clusters confined in zeolites. *Nat. Mater.* **15**, 1017.
14. G. Seifert (2004). Nanomaterials: Nanocluster magic. *Nat. Mater.* **3**, 77.
15. X. Yang, X. Chen, C. Zhang, X. Xie, B. Yang, B. Xu, D. Liu, and H. Yang (2016). Prediction of vapor–liquid equilibria for the Pb–X (X = Ag, Cu and Sn) systems in vacuum distillation using ab initio methods and Wilson equation. *Fluid Phase Equilib.* **417**, 25.
16. A. K. Sum and S. I. Sandler (1999). Use of ab initio methods to make phase equilibria predictions using activity coefficient models. *Fluid Phase Equilib.* **158–160**, 375.
17. S. Osmekhin, M. Tchaplyguine, M. H. Mikkelä, M. Huttula, T. Andersson, O. Björneholm, and S. Aksela (2010). Size-dependent transformation of energy structure in free tin clusters studied by photoelectron spectroscopy. *Phys. Rev. A* **81**, 023203.
18. M. Tchaplyguine, G. Öhrwall, T. Andersson, S. Svensson, O. Björneholm, M. Huttula, M. Mikkelä, S. Urpelainen, S. Osmekhin, A. Caló, S. Aksela, and H. Aksela (2014). Size-dependent evolution of electronic structure in neutral Pb clusters—As seen by synchrotron-based X-ray photoelectron spectroscopy. *J. Electron Spectrosc.* **195**, 55.
19. J. Bahn, P. Oelßner, M. Köther, C. Braun, V. Senz, S. Palutke, M. Martins, E. Rühl, G. Ganteför, T. Möller, B. von Issendorff, D. Bauer, J. Tiggesbäumker, and K. H. Meiwes-Broer (2012). Pb 4f photoelectron spectroscopy on mass-selected anionic lead clusters at FLASH. *New J. Phys.* **14**, 075008.
20. B. Wang, J. Zhao, X. Chen, D. Shi, and G. Wang (2005). Atomic structures and covalent-to-metallic transition of lead clusters Pb_n ($n = 2$–22). *Phys. Rev. A* **71**, 033201.
21. B. Assadollahzadeh, S. Schäfer, and P. Schwerdtfeger (2010). Electronic properties for small tin clusters Sn_n ($n \leq 20$) from density functional theory and the convergence toward the solid state. *J. Comput. Chem.* **31**, 929.
22. C. Majumder, V. Kumar, H. Mizuseki, and Y. Kawazoe (2001). Small clusters of tin: Atomic structures, energetics, and fragmentation behavior. *Phys. Rev. B* **64**, 233405.
23. C. Majumder, V. Kumar, H. Mizuseki, and Y. Kawazoe (2002). Ionization potentials of small tin clusters: first principles calculations. *Chem. Phys. Lett.* **356**, 36.
24. C. Majumder, V. Kumar, H. Mizuseki, and Y. Kawazoe (2005). Atomic and electronic structures of neutral and cation Sn_n ($n = 2$–20) clusters: A comparative theoretical study with different exchange-correlation functionals. *Phys. Rev. B* **71**, 035401.
25. T. Bachels and R. Schäfer (1999). Formation enthalpies of Sn clusters: a calorimetric investigation. *Chem. Phy. Lett.* **300**, 177.
26. S. Yahachi, Y. Kenzi, M. Kazuhiro, and N. Tamotsu (1982). Formation and Ionization Potentials of Lead Clusters. *Jpn. J. Appl. Phys.* **21**, L396.

27. C. Rajesh and C. Majumder (2007). Atomic and electronic structures of neutral and charged Pb_n clusters (n = 2–15): theoretical investigation based on density functional theory. *J. Chem. Phys.* **126**, 244704.
28. X. Li, W. Lu, C. Wang, and K. M. Ho (2010). Structures of Pb_n (n = 21–30) clusters from first-principles calculations. *J. Phys. Condens. Matter* **22**, 465501.
29. E. M. Sosa-Hernández, J. M. Montejano-Carrizales, and P. G. Alvarado-Leyva (2015). Stability and magnetic behavior of small Co_xSn_y ($x + y \leq 5$) atomic clusters. *J. Alloys Compd.* **632**, 772.
30. P. N. Samanta and K. K. Das (2012). Electronic structure, bonding, and properties of Sn_mGe_n ($m + n \leqslant 5$) clusters: A DFT study. *Comput. Theor. Chem.* **980**, 123.
31. E. M. Sosa-Hernández, J. M. Montejano-Carrizales, and P. G. Alvarado Leyva (2015). Geometrical shapes, stabilities and electronic behavior of small Fe_xSn_y ($x + y \leq 5$) atomic clusters. *Eur. Phys. J. D* **69**, 212.
32. T. B. Tai, N. M. Tam, and M. T. Nguyen (2011). Evolution of structures and stabilities of zinc-doped tin clusters Sn_nZn, n = 1–12. Three-dimensional aromaticity of the magic clusters $Sn_{10}Zn$ and $Sn_{12}Zn$. *Chem. Phys.* **388**, 1.
33. L. O. Paz-Borbon, A. Hellman, J. M. Thomas, and H. Gronbeck (2013). Efficient hydrogenation over single-site bimetallic RuSn clusters. *Phys. Chem. Chem. Phys.* **15**, 9694.
34. J. J. Melko, U. Werner, R. Mitric, V. Bonacic-Koutecky, and A. W. Castleman Jr. (2011). Electronic structure similarities in $Pb_xSb_y^-$ and $Sn_xBi_y^-$ clusters. *J. Phys. Chem. A* **115**, 10276.
35. X. Xing, Z. Tian, H. Liu, and Z. Tang (2003). Magic bimetallic cluster anions of M/Pb (M = Au, Ag and Cu) observed and analyzed by laser ablation and time-of-flight mass spectrometry. *Rapid Commun. Mass Spectrom.* **17**, 1411.
36. J. J. Melko, S. V. Ong, U. Gupta, J. U. Reveles, J. D'Emidio, S. N. Khanna, and A. W. Castleman (2010). Anion Photoelectron Spectroscopy and First-Principles Study of Pb_xIn_y Clusters. *J. Phys. Chem. C* **114**, 20907.
37. C. Rajesh and C. Majumder (2008). Structure and electronic properties of Pb_nM (M = C, Al, In, Mg, Sr, Ba, and Pb; n = 8, 10, 12, and 14) clusters: theoretical investigations based on first principles calculations. *J. Chem. Phys.* **128**, 024308.
38. S. Barman, C. Rajesh, G. P. Das, and C. Majumder (2009). Structural and electronic properties of $Sn_{n-1}Pb$ and $Pb_{n-1}Sn$ clusters: a theoretical investigation through first principles calculations. *Eur. Phys. J. D* **55**, 613.
39. S. Orel and R. Fournier (2013). Density functional theory and global optimization study of Sn_mPb_n clusters ($7 \leqslant m + n \leqslant 12$, $0 \leqslant m/(m + n) \leqslant 1$). *J. Chem. Phys.* **138**, 064306.
40. X. Huang, Y. Su, L. Sai, J. Zhao, and V. Kumar (2015). Low-Energy Structures of Binary Pt–Sn Clusters from Global Search Using Genetic Algorithm and Density Functional Theory. *J. Clust. Sci.* **26**, 389.
41. V. E. Bondybey, M. Heaven, and T. A. Miller (1983). Laser vaporization of tin: Spectra and ground state molecular parameters of Sn_2. *J. Chem. Phys.* **78**, 3593.
42. S. Yoshida and K. Fuke (1999). Photoionization studies of germanium and tin clusters in the energy region of 5.0–8.8 eV: Ionization potentials for Ge_n (n = 2–57) and Sn_n (n = 2–41). *J. Chem. Phys.* **111**, 3880.
43. C. Rajesh, C. Majumder, M. G. R. Rajan, and S. K. Kulshreshtha (2005). Isomers of small Pb_n clusters (n = 2–15): Geometric and electronic structures based onab initiomolecular dynamics simulations. *Phys. Rev. B* **72**, 235411.
44. M. E. Eberhart, R. C. O'Handley, and K. H. Johnson (1984). Molecular-orbital models of structural phase transformations in crystalline and amorphous cobalt alloys. *Phys. Rev. B* **29**, 1097.
45. Y. Bai, H. Cheng, H. Sun, N. Xu, and K. Deng (2011). Structures, stabilities and electronic properties of $FePb_n$ (n = 1–14) clusters: Density-functional theory investigations. *Physica B* **406**, 3781.
46. J. Wen, J. Zhang, G. Chen, X. Zhang, and Z. Wen (2016). Structure, stability and magnetic properties of $(NiAl)_n$($n \leq 6$) clusters. *J. Phys. Chem. Solids* **96–97**, 68.
47. F. Suo, Y. Zhang, and S. Huang (2017). Theoretical Investigation of Electronic Properties of Undoped and Ag-Doped $(CdTe)_{16\times N}$ Multi-cage Nanochains. *J. Clust. Sci.* **28**, 1393.
48. K. Li, C. Yang, M. Wang, and X. Ma (2017). Adsorption and Dissociation of H_2 on Cluster Al_6N. *J. Clust. Sci.* **28**, 1335.
49. Y. Jin, Y. Tian, X. Kuang, C. Zhang, C. Lu, J. Wang, J. Lv, L. Ding, and M. Ju (2015). Ab Initio Search for Global Minimum Structures of Pure and Boron Doped Silver Clusters. *J. Phys. Chem. A* **119**, 6738.

50. X. X. Xia, A. Hermann, X. Y. Kuang, Y. Y. Jin, C. Lu, and X. D. Xing (2016). Study of the Structural and Electronic Properties of Neutral and Charged Niobium-Doped Silicon Clusters: Niobium Encapsulated in Silicon Cages. *J. Phys. Chem. C* **120**, 677.
51. G. Li, J. Wang, X. Chen, Z. Zhou, H. Yang, B. Yang, B. Xu, and D. Liu (2017). Bimetallic Pb_nCu_n (n = 2–14) clusters were investigated by density functional theory. *Comput. Theor. Chem.* **1106**, 21.
52. Y. Jin, G. Maroulis, X. Kuang, L. Ding, C. Lu, J. Wang, J. Lv, C. Zhang, and M. Ju (2015). Geometries, stabilities and fragmental channels of neutral and charged sulfur clusters: S_n^Q (n = 3–20, Q = 0, ±1). *Phys. Chem. Chem. Phys.* **17**, 13590.
53. X. Xing, A. Hermann, X. Kuang, M. Ju, C. Lu, Y. Jin, X. Xia, and G. Maroulis (2016). Insights into the geometries, electronic and magnetic properties of neutral and charged palladium clusters. *Sci. Rep.* **6**, 19656.
54. W. G. Sun, J. J. Wang, C. Lu, X. X. Xia, X. Y. Kuang, and A. Hermann (2017). Evolution of the Structural and Electronic Properties of Medium-Sized Sodium Clusters: A Honeycomb-Like Na_{20} Cluster. *Inorg. Chem.* **56**, 1241–1248.